

Article

Green Biosynthesis of Zinc Oxide Nanoparticles Using *Pluchea indica* Leaf Extract: Antimicrobial and Photocatalytic Activities

Abdulaziz A. Al-Askar ¹, Amr H. Hashem ^{2,*} , Nadeem I. Elhussieny ^{3,4} and Ebrahim Saied ^{2,*} 

¹ Department of Botany and Microbiology, Faculty of Science, King Saud University, P.O. Box 2455, Riyadh 11451, Saudi Arabia

² Botany and Microbiology Department, Faculty of Science, Al-Azhar University, Cairo 11884, Egypt

³ Department of Life Science and Chemistry, Constructor University, 28759 Bremen, Germany

⁴ Institute of Environmental Biology and Biotechnology, University of Applied Sciences Bremen, Am Neustadtswall 30, 28199 Bremen, Germany

* Correspondence: amr.hosny86@azhar.edu.eg (A.H.H.); hema_almasry2000@yahoo.com (E.S.)

Abstract: Nanotechnology is playing a critical role in several essential technologies with nanoscale structures (nanoparticles) in areas of the environment and biomedicine. In this work, the leaf extract of *Pluchea indica* was utilized to biosynthesize zinc oxide nanoparticles (ZnONPs) for the first time and evaluated for antimicrobial and photocatalytic activities. Different experimental methods were used to characterize the biosynthesized ZnONPs. The biosynthesized ZnONPs showed maximum Ultraviolet–visible spectroscopy (UV-vis) absorbance at a wavelength of 360 nm. The X-ray diffraction (XRD) pattern of the ZnONPs exhibits seven strong reflection peaks, and the average particle size was 21.9 nm. Fourier-transform infrared spectroscopy (FT-IR) spectrum analysis reveals the presence of functional groups that help in biofabrication. The existence of Zn and O was confirmed by the Energy-dispersive X-ray (EDX) spectrum and the morphology by SEM images. Antimicrobial studies showed that the biosynthesized ZnONPs have antimicrobial efficacy against *Escherichia coli*, *Pseudomonas aeruginosa*, *Enterococcus faecalis*, *Bacillus subtilis*, *Staphylococcus aureus*, *Candida albicans* and *Cryptococcus neoformans* where inhibition zones at concentration 1000 µg/mL were 21.83 ± 0.76, 13.0 ± 1.1, 14.9 ± 0.85, 24.26 ± 1.1, 17.0 ± 1.0, 20.67 ± 0.57 and 19.0 ± 1.0 mm respectively. Under both dark and sunlight irradiation, the photocatalytic activity of ZnONPs was evaluated towards the degradation of the thiazine dye (methylene blue-MB). Approximately 95% of the MB dye was broken down at pH 8 after 150 min of sunlight exposure. The aforementioned results, therefore, suggest that ZnONPs synthesized by implementing environmentally friendly techniques can be employed for a variety of environmental and biomedical applications.

Keywords: green biosynthesis; zinc oxide nanoparticles; antimicrobial activity; photocatalytic activity



Citation: Al-Askar, A.A.; Hashem, A.H.; Elhussieny, N.I.; Saied, E. Green Biosynthesis of Zinc Oxide Nanoparticles Using *Pluchea indica* Leaf Extract: Antimicrobial and Photocatalytic Activities. *Molecules* **2023**, *28*, 4679. <https://doi.org/10.3390/molecules28124679>

Academic Editor: Periakaruppan Prakash

Received: 18 May 2023

Revised: 31 May 2023

Accepted: 5 June 2023

Published: 9 June 2023



Copyright: © 2023 by the authors. Licensee MDPI, Basel, Switzerland. This article is an open access article distributed under the terms and conditions of the Creative Commons Attribution (CC BY) license (<https://creativecommons.org/licenses/by/4.0/>).

1. Introduction

The printing and dyeing industries are among the worst environmental offenders because they release a lot of dyes into wastewater [1]. These dyes are not only unattractive but also dangerous to the environment and living things when present in rivers [2]. The textile industry is now required to remove dyes from its released wastewater due to increasingly stringent environmental regulations. Controlling dye effluent output, however, has proven difficult over time. According to reports, over 7×10^5 tons of dyes are produced annually for synthetic items, with a global yearly output of around 80 million tons [3]. These dyes seriously damage the environment, even when only trace amounts are emitted. Methylene blue is the synthetic dye most frequently used in the textile industry to color textiles [4,5]. Because of the strength of the MB dye molecules, they are difficult for a standard wastewater treatment procedure to break down [6]. MB dye also poisons serotonin and the central nervous system severely [7]. Multiple pathways may be responsible for photocatalyst deactivation, according to the literature that is currently available. In order

to change the surface characteristics of the photocatalysts, the aqueous substances may first bind to them through covalent bonds, electrostatic effects, interaction, and secondary bonds. Second, the altered surface charge may cause the photocatalysts to aggregate, and a strong adsorbate–surface contact may cause the photocatalysts to dissolve [8]. Numerous studies have shown that exposure to dye-contaminated water can cause damage to various organs, including the thyroid, conjunctiva/cornea, brain, kidney, liver, gastrointestinal tract, and reproductive system [9–11]. Therefore, in today’s dye wastewater treatment, effective dye removal is a hotly debated topic. The contamination brought on by dye effluent has increased interest in its biological, chemical, and physical remediation. The most popular techniques for sequestering and decolorizing dyes are adsorption, coagulation–flocculation, ion exchange, catalytic degradation, chemical precipitation, and ion exchange [2,12,13]. In order to reduce dangerous pollutants in indoor air, many techniques, such as biological degradation, thermal and non-thermal plasma treatment, membrane separation, and photocatalytic oxidation (PCO), have been investigated to date. However, photocatalytic oxidation still has drawbacks, such as quick catalyst deactivation, lower effectiveness under typical working conditions, and the formation of undesirable byproducts [14]. However, these traditional techniques offer some disadvantages, such as limited efficiency, high costs, and unintended side effects [15]. Materials used in photocatalytic activity ought to be safe and resistant to photo-oxidative degradation. Nanotechnology is concerned with creating materials at the nanoscale, which ranges from 1 to 100 nm. In comparison to bulk, the material’s nanoscale size dimension displayed optimal physicochemical characteristics [16,17]. Nanomaterials have generated a lot of attention because of the many applications they have in fields as diverse as medicine, biotechnology, the food industry, agriculture, transportation, national security, sensors, packaging, information technology, aerospace, textiles, and cosmetics [18–25]. Due to their successful applications in key disciplines such as catalysis, advanced nanomaterials have gained more researchers’ interest recently [26,27]. Adsorption, however, is a dependable dye removal method that is operationally easier, economically feasible, highly effective, and has a strong regeneration capacity [28]. Additionally, this technique is renowned for being simple, flexible, and easy to utilize. Infectious illnesses, which cause a large number of deaths globally, are another big issue facing the medical industry [29]. Many dangerous microbes that cause numerous illnesses have been detected in dying wastewater. In addition, improper use of antibiotics and a lack of scientific resources to create such medications have resulted in mutations and generations of microorganisms that are resistant to them [30]. In order to prevent the spread of diseases and give a fresh perspective on therapy, it was important to look for novel therapeutic approaches, such as the use of nanotechnology. At low concentration levels (ppb–ppm), conventional semiconductor nanoparticles frequently exhibit poor pollutant adsorption capacities [14]. As an important micronutrient, zinc (Zn) is a key component of all six types of enzymes, which include oxidoreductases, lyases, isomerases, transferases, hydrolases, and ligases. It also plays a key role in many essential metabolic processes, including the manufacture of photosynthetic pigments [31]. Zinc protects membranes from oxidative and peroxidative damage by maintaining membrane integrity and stabilizing permeability. One of the most significant metal oxides, ZnO nanoparticles, have unique therapeutic effects as well as fungicidal, antibacterial, and catalytic capabilities. ZnONPs may be produced using a variety of methods, such as hydrothermal, solvothermal, chemical, sonication, precipitation, microwave, etc., but in modern times, a biological synthesis of ZnONPs using plant-derived products is widely employed [32–34]. ZnO nanoparticles are more effective at blocking UV radiation than bulk ZnO due to their high surface area-to-volume ratio [33]. There are several metabolites present in fungal biomass extracts that easily convert the precursor molecule to zinc ions and then to ZnONPs [35]. *Pluchea indica* Less., a member of the Asteraceae family, is a dual-purpose plant that is mostly found in tropical and subtropical areas. According to chemical analysis results, flavonoids, thiophenes, quinic acids, and other phenolic acids are this plant’s primary ingredients [36]. The most prevalent dietary polyphenolic chemicals among them are quinic acids, which are

abundantly present in tea, coffee, and other foods. Numerous bioactivities, including anti-inflammatory and hepatoprotection, have been documented [37]. Furthermore, *P. indica*'s high concentration of phenolic chemicals has led to research into and certification of its free radical scavenging capacity, which revealed that it has an antioxidation impact [38]. Herein, this study aims to biosynthesize ZnONPs using *P. indica* leaf extract for the first time, which is easy to use, ecofriendly, and safe. Moreover, the study aims to characterize biosynthesized ZnONPs by numerous techniques. Finally, to assess the antimicrobial activity and photocatalytic degradation.

2. Results and Discussion

2.1. Biosynthesis of ZnONPs Using Leaf Extract of *P. indica*

Since they are inexpensive and require minimal maintenance, plants are regarded as nature's chemical factories. Many plant parts, including fruit, leaves, stems, and roots, have frequently been used for the green production of nanoparticles because of the large phytochemicals they produce [39]. Iron, gold, silver, zinc oxide, and other nanoparticles have all been created simply using environmentally friendly methods [40]. Metallic ion bioreduction is caused by phytocompounds such as polyols, terpenoids, and polyphenols that are present in plant extracts [41]. As a result, efforts to synthesize ZnONPs using various techniques have intensified. In the current study, ZnONPs were made using a green process that is quick, easy, environmentally friendly, and economically feasible. Zinc ions were reduced, capped, and stabilized using leaf extracts of *P. indica*. To reduce the drawbacks associated with chemical and physical procedures, green approaches (plants, fungi, bacteria, actinomycetes, and yeasts) are chosen for the manufacture of metal and metal oxide NPs [42]. In this instance, the biocatalyst for reducing zinc ions to generate ZnONPs was the leaf extract of *P. indica*. The color change of the extract from pale green to turbid white after mixing with Zn (CH₃COO)₂·2H₂O indicates the formation of ZnONPs. This color shift is a result of the NPs' surface plasmon resonance becoming excited [43]. According to Fouda et al. [43], the formation of white ZnONPs was achieved by mixing the aqueous extract of *U. fasciata* with the zinc acetate solution. On the other hand, the biosynthesis of ZnONPs was performed by using *Delphinium uncinatum*, which was utilized for its anti-aging, cytotoxic, antibacterial, anti-diabetic, and anti-inflammatory properties. Llashin et al. [44] used *Ziziphus spina-christi* for the green biosynthesis of ZnONPs and selenium nanoparticles.

2.2. Characterization of ZnONPs

The precipitate's hue shifting to white indicates the presence of ZnONP. In order to find the maximal surface plasmon resonance, the absorbance of the generated color was measured in the 200–600 nm range. After 24 h, the greatest SPR for biosynthesized ZnONPs was recorded at 360 nm (Figure 1). According to Majhi and Kuiru [45], the metal-dielectric constant, the size, and form of the metal NPs, the surrounding medium, and the frequency of the SPR are all variables that affect its width. Earlier studies on the green manufacturing of ZnONPs revealed peak values between 320 and 380 nm [46]. The UV-visible absorption spectra of the biosynthesized ZnONPs from *Vernonia cinerea* leaf extract are 360 nm, which is the same result as that reported by Azim et al. [47]. Kumar et al. [48] found an absorbance peak at the resonance wavelength of 270 nm, which confirmed the existence of ZnONPs in the aqueous solution. According to Vijayakumar et al. [49], the UV spectra of Ae-ZnONPs include two peaks located at 275 and 380 nm, respectively. According to Shubha et al. [50], hexagonal ZnO NPs had an absorption maximum of 368 nm. Additionally, the zinc acetate was successfully transformed into the end product (ZnONPs), as evidenced by the maximum SPR being recorded at 380 nm. [51].

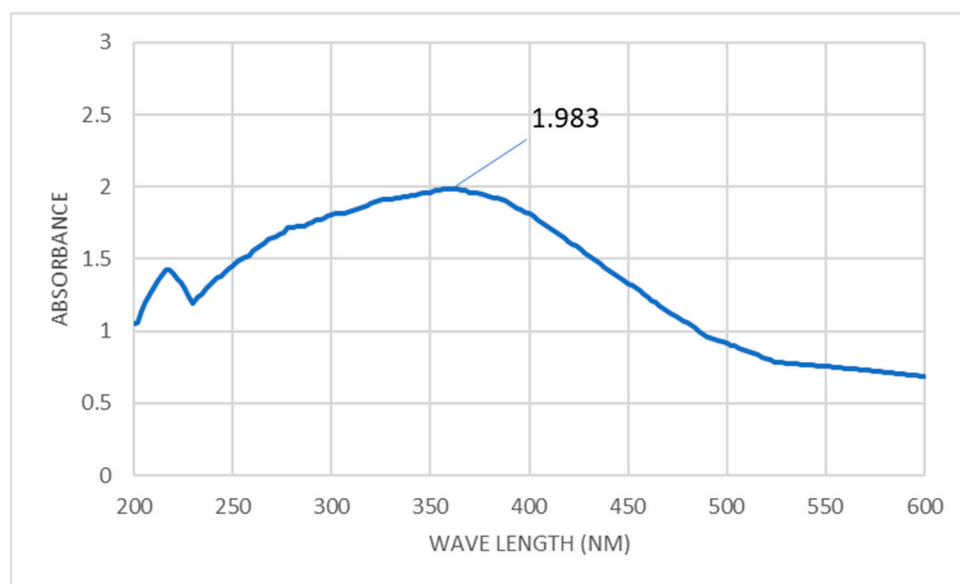


Figure 1. UV-vis spectra of biosynthesized ZnONPs at wavelength 200–800 nm.

FT-IR analysis was used to determine the different functional groups present in the cell-free filtrate and their functions in creating and stabilizing ZnONPs. As seen in Figure 2, the FT-IR chart exhibits peaks at certain wave numbers, 3331, 2895, 1775, 1622, 1427, 1368, 1315, 1203, 1159, 1107, 1053, 1031, 663, 611, 594, 556, 459, 445, and 414 cm^{-1} . The wide peak at 3331 cm^{-1} indicates the presence of the -OH group [52], whereas the observed peak at 2895 cm^{-1} represents the aldehyde group (CHO) [48]. Conversely, the peak bands at 1622, 1427, 1368, 1315, 1203, 1159, and 1107 cm^{-1} are related to the current carbonyl group (C=O), C-N bonds in aromatic stretching, and C-O [53–55]. The peaks of the NPs were variable during biosynthesis. At peaks of 400 to 600 cm^{-1} , as previously reported [50,56,57], the successful synthesis of ZnONPs was verified. Final confirmation of the zinc oxide bond comes from the band seen at 414 cm^{-1} . The information gathered confirmed the occurrence of a variety of functional groups, such as alkanes, alkenes, aliphatic, aromatic amines, and alkyls, which are present in the leaf extract of *P. indica* and are crucial for the stabilization, capping, and reduction of ZnONPs. Similar results were obtained by Dias et al. [58], who found that FT-IR analysis revealed a strong peak at 432.05 cm^{-1} , showing the characteristic Zn-O bond. For the zinc oxide nanoparticles produced using a green approach, Al-Dhabi and Arasu [59] achieved a peak of 417 cm^{-1} . Rajivgandhi et al. [60] have identified the peaks for the ZnO nanoparticle in the 400–4000 cm^{-1} wavelength region that was made using *Streptomyces enisocaesilis*.

The investigation of the morphological properties of synthesized NPs, such as their size, aggregation, and shape, may be performed with the use of transmission electron microscopy (TEM). As shown, phytochemicals produced by *P. indica* can reduce or cap zinc acetate and create spherical, widely scattered ZnONPs (Figure 2A,B). The average diameter of biosynthesized ZnONPs was 12.0 ± 2.2 nm, with sizes ranging from 6 to 21 nm. Figure 2B displayed the ZnONPs' area selected electron-diffraction (SAED) patterns, which exhibited good sharp rings and demonstrated the crystal structure of the ZnONPs. Spherical ZnONPs were successfully generated using the marine macroalgae *Ulva fasciata* Delile, with an average size of 10.62 nm and a size range of 3–33 nm [61]. Additionally, Abdo et al. [51] created spherical ZnONPs with diameters ranging from 6 nm to 21 nm. Numerous factors, including surface features, size, coating or capping agent, shape, reactivity, and solubility, can affect the activity of NPs [62]. Additionally, Aziz et al.'s [63] production of zinc oxide nanoparticles with a spherical shape and a size range of 28 to 42 nm was successful. However, Rajivgandhi et al.'s [60] synthesis of ZnONPs showed the diameter of the nanoparticle varying between 199 and 326 nm for the HP05 sample and between

12 and 35 nm for the HP01 sample. These findings lead us to assume that the synthesized ZnONPs used in the current work would have high activity due to their reduced sizes.

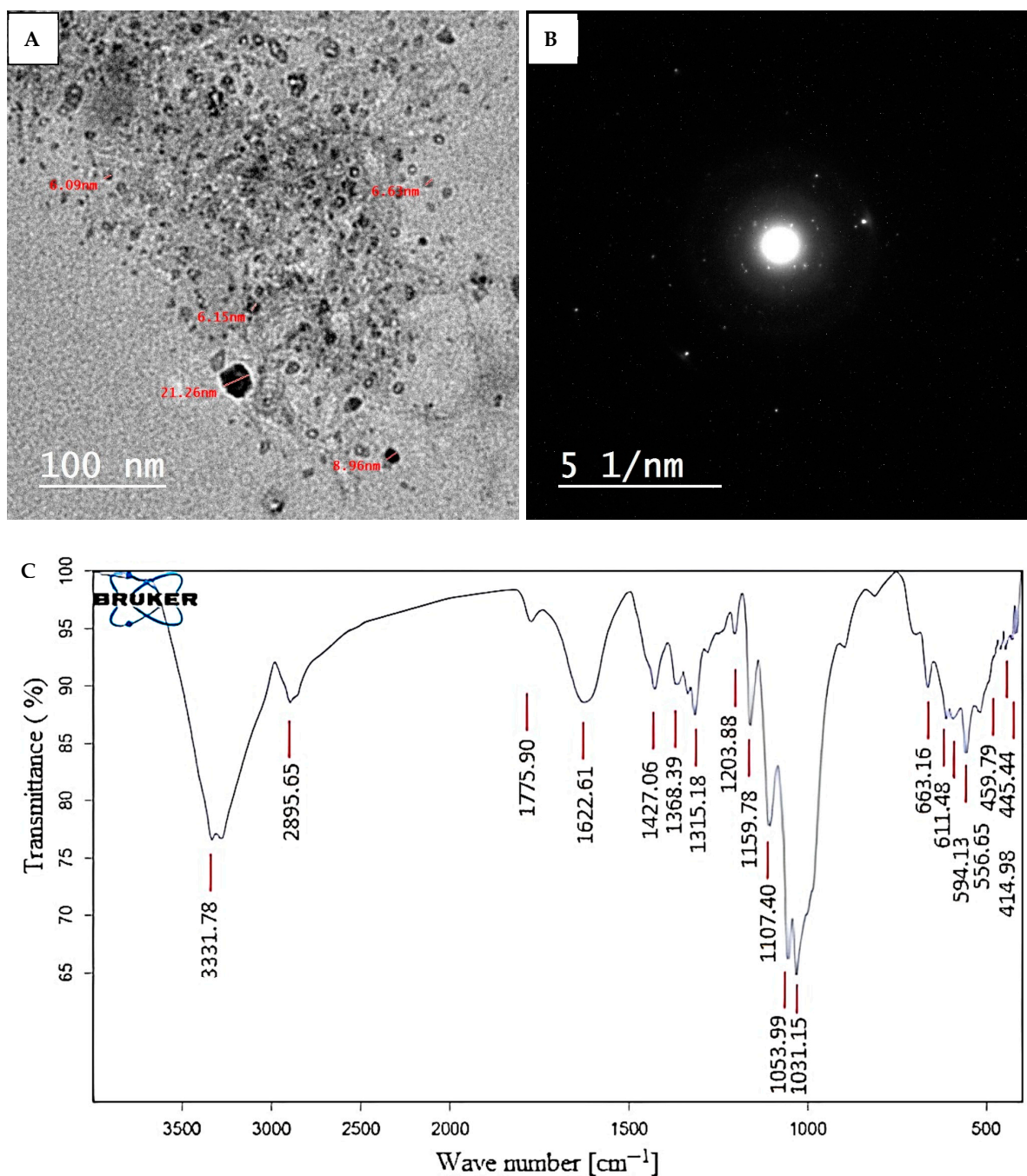


Figure 2. Characterization of biosynthesized ZnONPs. (A) TEM image; (B) SAED pattern; (C) FT-IR spectra.

Particle size and size distribution investigations may be performed using a variety of approaches. Dynamic light scattering (DLS) is one such well-liked method for figuring out the particle size and size distribution of nanoparticles. The average particle size, distribution, and polydispersity index are calculated by Brownian motion by measuring the light scattering. The analysis revealed that the average particle size of the biosynthesized zinc oxide nanoparticles was 50.7 nm, and their PDI was 0.31. Figure 3B displays the size distribution of intensity. Similarly, the particle size analysis was performed for zinc oxide nanoparticles, which are synthesized by *Cordyceps militaris* [58]. According to Mohamed

et al. [52], the obtained ZnONPs were poly-dispersed mixtures with average diameters of 135.5 nm (86.4%) and 163.34 nm (92.7%) for nanorod and hexagonal ZnONPs, respectively.

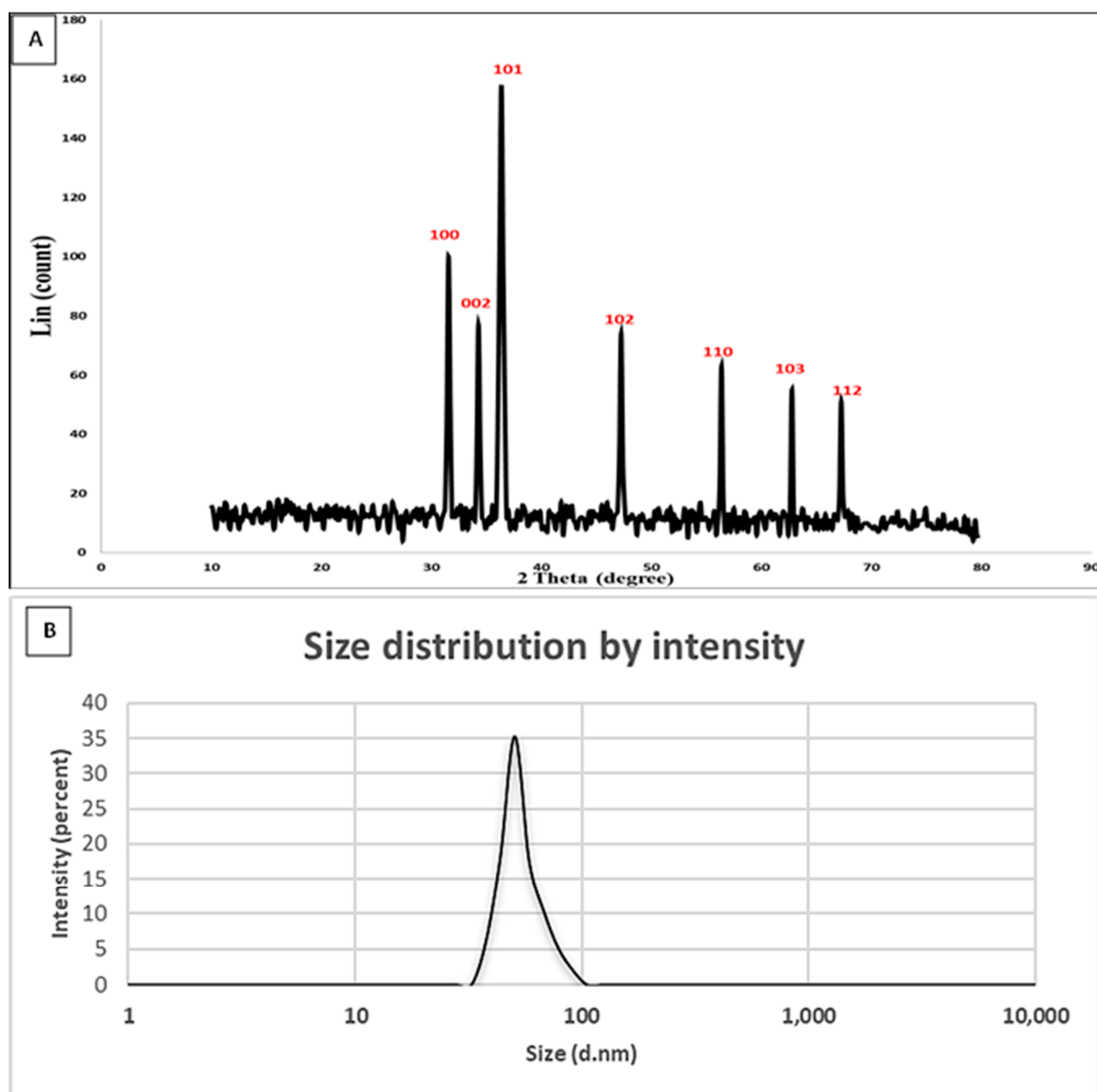


Figure 3. (A) XRD analysis, (B) DLS analysis of biosynthesized ZnONPs.

By using XRD, the crystallinity of biosynthesized ZnONPs in the range of two theta values was examined (Figure 3A). The spectra show the existence of seven prominent peaks for Bragg reflection at (100), (002), (101), (102), (110), (103), and (112) at two theta values of 31.6° , 34.3° , 36.2° , 47.2° , 56.4° , 62.8° , and 67.2° , respectively. According to the Diffraction Standards JCPDS data (Zincite, JCPDS 5-0664) for polycrystalline wurtzite structure, the collected results demonstrated the crystallinity of ZnONPs [64]. The XRD pattern for the crystalline nature of biologically produced ZnONPs was consistent with our observations [51,52]. The particle size of the created NPs was determined using the Debye-Scherrer equation. The average ZnONP size that could be analyzed by TEM in this instance was 21.9 nm, and the FWHM (2θ) value was 0.3981. The effective manufacturing of small ZnONPs of the previously reported sizes is indicated by the widening of the bases of Bragg's diffraction peaks [58,64]. The different peaks recently approximated the diffraction

planes (100), (260), (002), (101), (102), and (101). The findings support the biofabricated ZnONPs' wurtzite structure [47].

The surface appearance and qualitative and quantitative elemental compositions of ZnONPs produced by *P. indica* leaf extract were examined using SEM in conjunction with EDX equipment. As shown, the produced ZnONPs had a spherical form and were evenly spread (Figure 4A). The synthesis of ZnONPs was successful, as seen by the prominent peak in the zinc area of the EDX chart (Figure 4B). According to the EDX chart, Zn makes up a large portion of the synthesized components. Figure 4B demonstrates the presence of C, O, and Zn, with weight percentages of 20.5, 29.3, and 50%, respectively. The ZnO nanoparticle's elemental composition showed that it included 61.57% oxygen and 38.43% zinc, respectively, according to Rajivgandhi et al. [60]. In a manner similar to this, ZnONPs were produced using *Zingiber officinale* root extract and then analyzed using EDAX. Additionally, elemental analysis of nanoparticles generated from root extract showed that they included around 80% zinc and 19% oxygen [65]. Furthermore, *S. marginatum* and *U. lactuca* produced ZnONPs that were mostly composed of Zn and O with weight percentages of (51.6 and 48.4%) and (48.3 and 51.7%), respectively [61]. Similar to this, Mohamed et al. [66] discovered that Zn (58.3%) and O (20%) were the two main peaks of the EDX spectra for ZnONPs generated by *P. chrysogenum*, in addition to the occurrence of other peaks linked to biomolecules in *P. chrysogenum* filtrate that conjugated with ZnONPs.

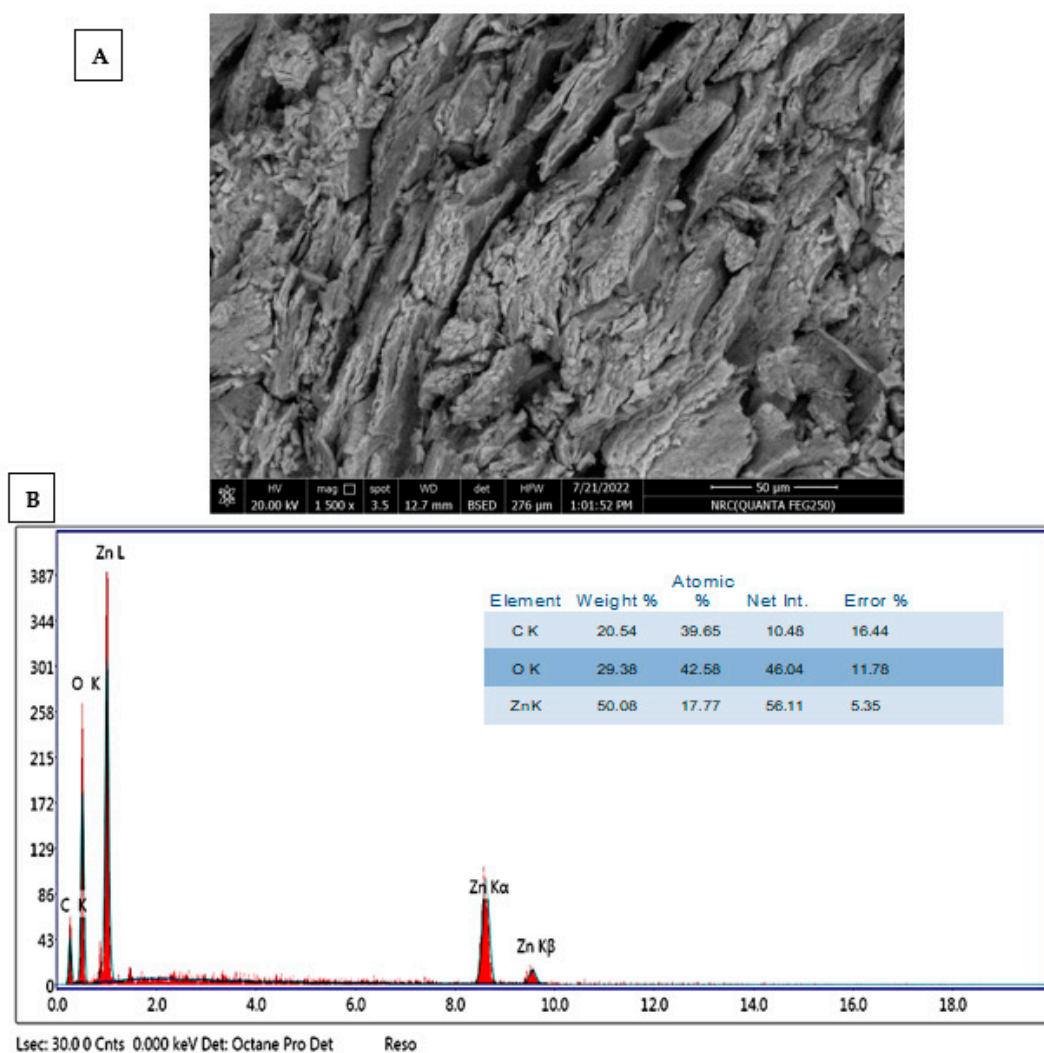


Figure 4. (A) Scanning Electron Microscope (SEM) of ZnONPs; (B) EDX spectrum showed elemental compositions of biosynthesized ZnONPs.

2.3. Antimicrobial Activity

Zinc oxide nanoparticles have piqued the interest of researchers and scientists during the last decade due to their numerous potential applications in biomedicine, the environment, and electronics. ZnO nanoparticles are of tremendous interest because of their low cost, safety, and ease of manufacture. In the current study, the biosynthesized ZnONPs using leaf extract of *P. indica* were assessed as antimicrobial agents against Gram-positive and Gram-negative bacteria as well as unicellular fungi, as shown in Table 1. Results displayed that the biosynthesized ZnONPs exhibited antibacterial activity where inhibition zones were 21.83 ± 0.76 , 13.0 ± 1.1 , 14.9 ± 0.85 , 24.26 ± 1.1 , and 17.0 ± 1.0 mm toward *E. coli*, *P. aeruginosa*, *E. faecalis*, *B. subtilis* and *S. aureus* respectively, at a concentration of 1000 $\mu\text{g}/\text{mL}$. Moreover, *B. subtilis* was the most sensitive among tested bacterial strains to ZnONPs, where the MIC was 62.5 $\mu\text{g}/\text{mL}$, while *P. aeruginosa* was the least sensitive, where the MIC was 500 $\mu\text{g}/\text{mL}$. Compared to standard antibiotic (SAM), SAM showed weak antibacterial activity against all tested bacterial strains, where MICs were in the range of 500–1000 $\mu\text{g}/\text{mL}$. Furthermore, the biosynthesized ZnONPs revealed potential antifungal activity against *C. albicans* and *C. neoformans* where inhibition zones at concentrations of 1000 $\mu\text{g}/\text{mL}$ were 20.67 ± 0.57 and 19.0 ± 1.0 mm, respectively. Moreover, the MIC was 125 $\mu\text{g}/\text{mL}$ for both *C. albicans* and *C. neoformans*. Although no previous studies on the biosynthesis of ZnONPs by *P. indica* leaf extract, previous studies reported that leaf plant extracts were used for the biosynthesis of ZnONPs [67,68]. Naseer, Aslam, Khalid, and Chen [67] succeeded in the biosynthesis of ZnONPs using leaf extracts of *Cassia fistula* and *Melia azadarach*, where these nanoparticles showed promising antibacterial activity against *E. coli* and *S. aureus*. Moreover, [69] reported that ZnONPs synthesized by leaf extracts of *Passiflora caerulea* revealed antimicrobial activity toward urinary tract infection-causing microbes. Moreover, Gharpure et al. [70] illustrated that leaf extract of *Neolamarckia cadamba* can be used for the green biosynthesis of ZnONPs and also found that these nanoparticles have antibacterial activity against *B. subtilis*, *S. aureus*, *P. aeruginosa*, and *E. coli*. Furthermore, *Pisonia alba* leaf extract was used for ZnONPs biosynthesis and exhibited potential antibacterial activity toward Gram-negative and Gram-positive bacteria [71]. Additionally, Chaudhary et al. [72] succeeded in the biosynthesis of ZnONPs using *Aloe vera* peel extract and found ZnONPs have promising antimicrobial activity against *E. coli* (MTCC-41) and *A. niger* (MTCC-404). Bala et al. [73] reported that the biosynthesized ZnONPs using leaf extracts of *Hibiscus subdariffa* had antibacterial activity toward *S. aureus* and *E. coli*. Moreover, ZnONPs were green biosynthesized using cinnamon and bay leaves and displayed antibacterial and antifungal activity against *S. aureus*, *S. epidermidis*, *E. coli*, *Klebsiella pneumoniae*, and *C. albicans*. Moreover, ZnONPs were biosynthesized through a green and eco-friendly method, where *Allium sativum* and *Zingiber officinale* extracts were used, and the biosynthesized ZnONPs showed antibacterial activity against *E. coli*, *P. putida*, *S. aureus*, and *Streptococcus pyogenes* [74]. The production of reactive oxygen species (ROS), such as hydroxyl radicals (OH), hydrogen peroxide (H_2O_2), and peroxide (O_2), may be the cause of the antibacterial activity of biosynthesized ZnONPs. A number of processes have been linked to ROS, including the internalization of NPs as a result of proton motive force loss, cell wall disintegration brought on by ZnO-localized contacts, enhanced membrane permeability, and the consumption of dangerous dissolved zinc ions. These have led to oxidative stress-related gene expression, intracellular outflow, and mitochondrial malfunction, which have suppressed cell development and led to cell death [75]. Dwivedi et al. [76] conducted research on the mechanism of ZnO-NPs' antibacterial action, which they determined to be ROS production as a result of treatment with DCFH-DA dye. When the dye enters the bacterial cell passively, cell esterases break it down, releasing DCFH. Reactive oxygen species (ROS) enable the oxidation of DCFH to DCF, a highly fluorescent chemical known as dichlorofluorescein. The amount of reactive oxygen species (ROS) is correlated with the intensity of the fluorescent signal, which was quantified using flow cytometry or a microplate reader [77].

Table 1. Antimicrobial activity of biosynthesized ZnONPs.

Microbial Strains	<i>P. indica</i> Leaf Extract	Zinc Acetate	ZnO NPs		SAM/NS **	
	IZ/mm *	IZ /mm	IZ/mm	MIC	IZ	MIC
<i>E. coli</i>	ND	ND	21.83 ± 0.76 ^{ab}	125	12.5 ± 0.5 ^b	500
<i>P. aeruginosa</i>	ND	ND	13.0 ± 1.1 ^f	500	9.33 ± 0.57 ^c	1000
<i>E. faecalis</i>	ND	ND	14.9 ± 0.85 ^{ef}	500	12.5 ± 0.86 ^b	500
<i>B. subtilis</i>	ND	ND	24.26 ± 1.1 ^a	62.5	15.4 ± 0.53 ^a	125
<i>S. aureus</i>	ND	ND	17.0 ± 1.0 ^{de}	250	9.73 ± 0.46 ^c	1000
<i>C. albicans</i>	ND	ND	20.67 ± 0.57 ^{bc}	125	11.83 ± 0.76 ^b	500
<i>C. neoformans</i>	ND	ND	19.0 ± 1.0 ^{cd}	125	10.16 ± 0.29 ^c	1000

* IZ means inhibition zone, ** SAM/NS means Ampicillin–sulbactam/nystatin. Letters ^{a,b,c,...} mean significance power.

2.4. Photocatalytic Degradation of Methylene Blue-MB Using ZnONPs

Either directly applying high-energy light sources to the surface of the nanomaterials or utilizing a photosensitization approach is used in the degradation process. Nanoparticles are irradiated with light, and direct photocatalytic degradation happens when electrons are moved from the valence band (filled) to the conduction band by the use of light energy. This process is known as photo-excitation [78]. In order to undertake a comparative analysis, the potential of ZnONPs for the decolorization of methylene blue dye was examined in this work at various ZnONPs concentrations (25, 50, 75, and 100 mg) for various contact durations (30, 60, 90, 120, 150, 180, 240, and 300 min) in both light and dark. The data analysis showed the dosage and time dependence of ZnONPs' catalytic activity. Surprisingly, exposure to light accelerated the biodegradation of ZnONPs more than exposure to darkness (Figure 5A–D). In comparison to the control, which had a decolorization percentage of $9.1 \pm 0.35\%$ after 240 min. The decolorization percentages at 0.25 mg mL^{-1} the concentration of ZnONPs reached up to $30.5 \pm 0.51\%$ and $15.7 \pm 0.72\%$ under sunlight and dark conditions, respectively. At 0.5 mg mL^{-1} of ZnONPs, the decolorization percentages under sunlight stimulation increased to $51.8 \pm 1.04\%$ after 240 min. After 180 min, the percentages of decolorization at 0.75 mg mL^{-1} of ZnONPs under light and dark conditions were $77.2 \pm 0.34\%$ and $40.3 \pm 0.84\%$, respectively. In the presence of sunlight, the maximum decolorization was attained at 1.0 mg mL^{-1} of ZnONPs with percentages of $95.3 \pm 0.65\%$ after 150 min; while in the absence of sunlight at the same NPs concentration, the decolorization was $56.3 \pm 0.93\%$ after 180 min. These findings showed that 1.0 mg mL^{-1} of ZnONPs after 150 min of contact time was the most suitable condition. Saied et al. [79] found that the presence of light stimulators is necessary for the biosynthesized Hem-NPs to effectively degrade CV dye. An increase in ZnONPs concentration results in the greatest dye decolorization because there are more adsorption sites on the NPs' surface [80]. When compared to complicated solutions made up of many dye types or unidentified compounds, the time needed to decolorize and degrade either pure or one dye was the same [81]. The amount of dye that degrades is reducing as dye molecules compete for binding to the few available reaction sites on the nanoparticles at a greater concentration [80]. The number of active sites on the surface of the zinc oxide nanoparticles reduces as the amount of adsorbent increases, which lowers the adsorbent's capacity for the adsorption of dye molecules on its surface [82]. The photocatalytic efficiency of ZnONPs revealed higher eco-bioremediation capacities by degrading methylene blue (88.93%) and crystal violet (80.69%) dyes, according to Omran [83]. Additionally, Nguyen et al. [84] showed that the maximal Congo red dye degradation efficiency was 94.85% at 5.0 mg L^{-1} of ZnFe₂O₄@ZnO nanocomposites concentration and 0.33 g L^{-1} of ZnO dosage. Additionally, after 75 min of exposure to sunlight, almost 80% of the MB dye began to break down at pH 8 [85]. The

mycosynthesized ZnO nanoparticles showed potential dye degradation efficiency of up to 90% of fast green dye under photo illumination [48].

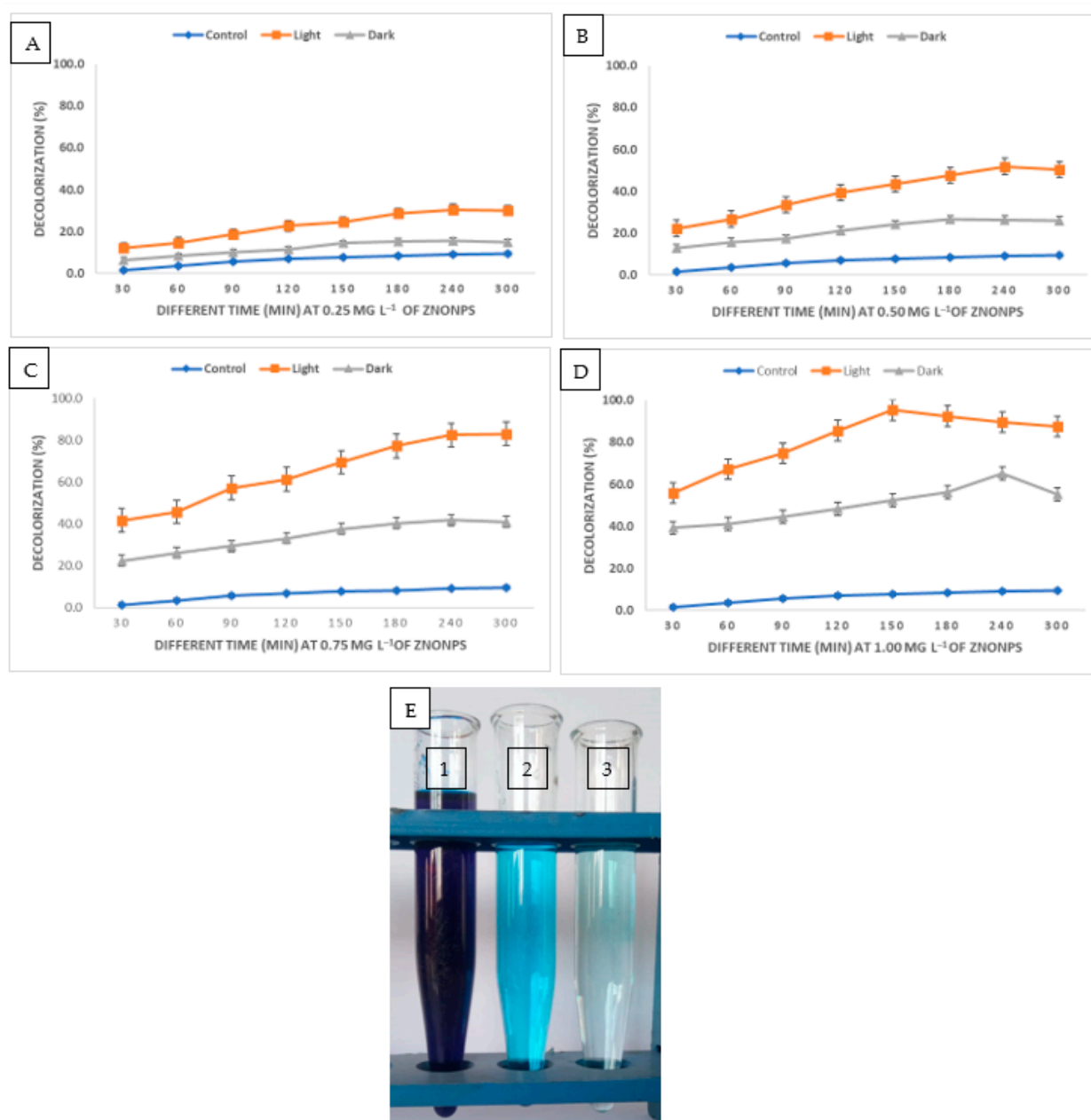


Figure 5. Decolorization percentages of MB dye under various stimulation settings (dark and sun-light), at various ZnONPs concentrations, and over various contact periods (A–D). Dye decolorization in dark and light environments (E) (1–3), where E1 represented the dye control, E2 represented the dye in the dark environment, and E3 represented the dye in the light environment.

One of the most crucial pieces of knowledge to have while creating a system is the mechanism of adsorption. The major mechanism at play between the adsorbent and the adsorbed dye was electrostatic contact. In the adsorption process between the surfaces of the ZnONPs and dye, hydrogen bonds, hydrophobic interactions, and interactions of the ZnO-NPs with the aromatic rings of the dye all played important roles. Additionally, the C=O, OH, NH, and phenyl groups of the ZnONPs, which served as adsorption sites, interacted with the aromatic rings of dye molecules [86]. Zinc oxide is essentially insoluble in aqueous solutions and functions as a flimsy base. ZnONPs' valence band electrons are photoexcited into their conduction band by sunlight. O₂ was converted into O₂^{•-} radicals,

which were subsequently converted into hydroxyl radicals as a result of the separation of charges brought on by the electrons in the conduction band. Additionally, the generated hole (h^+) has a propensity to split water molecules into hydrogen (H^+) ions and hydroxyl radicals (OH^\bullet) (Figure 6). As a potent oxidizing agent, the generated hydroxyl radical (OH^\bullet) is extremely reactive and may be used to degrade dyes and other contaminants [87–89].

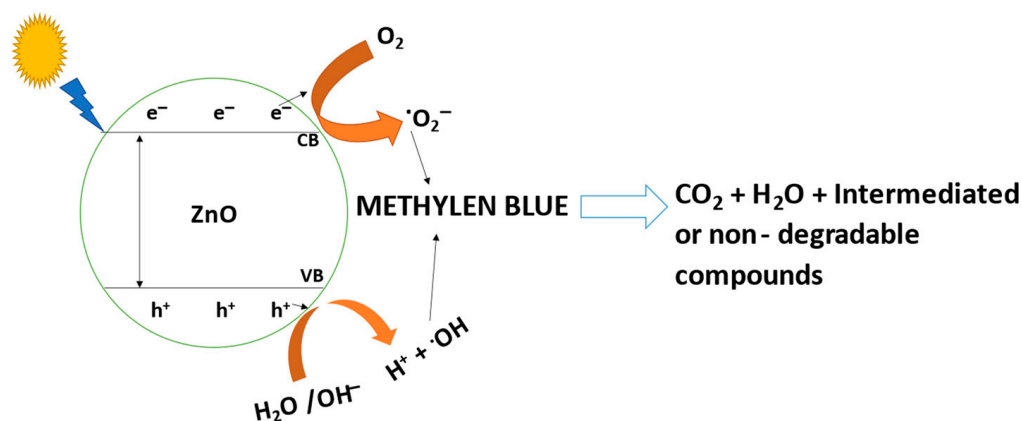
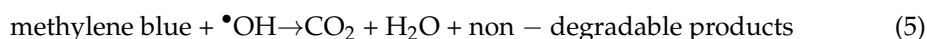


Figure 6. Flowchart showing the mechanism for decolorization and degradation of methylene blue dye by ZnONPs.

2.5. Reusability of ZnO Nanoparticles as Catalyst

In this work, the stability of biosynthesized ZnONPs for reuse in dye wastewater treatment was investigated. In this study, the regeneration of the employed ZnO nanoadsorbents from the dye solutions was carried out to ensure the appropriateness of our systems from the standpoint of industrial applications. ZnONPs were washed with a suitable proportion of water and ethanol for the concerned purpose after being centrifuged out of the dye solutions that had been treated. To make powdered ZnONPs, the sediment pellets were dried in an oven. In a similar way, ZnONPs were tested for reusability. Even after the fourth cycle of reusability, the dye removal percentage using ZnONPs showed a removal of 74.7% (Figure 7A,B). After four reuses, the dye removal efficiency was 87%, according to Rasool et al. [80]. These findings are consistent with other studies [87,90,91]. The unavoidable decrease in catalyst performance was mostly caused by the reduction of the catalytic site, the concentration of metal leaching, and the adsorption of intermediate products on the catalytic site [79].

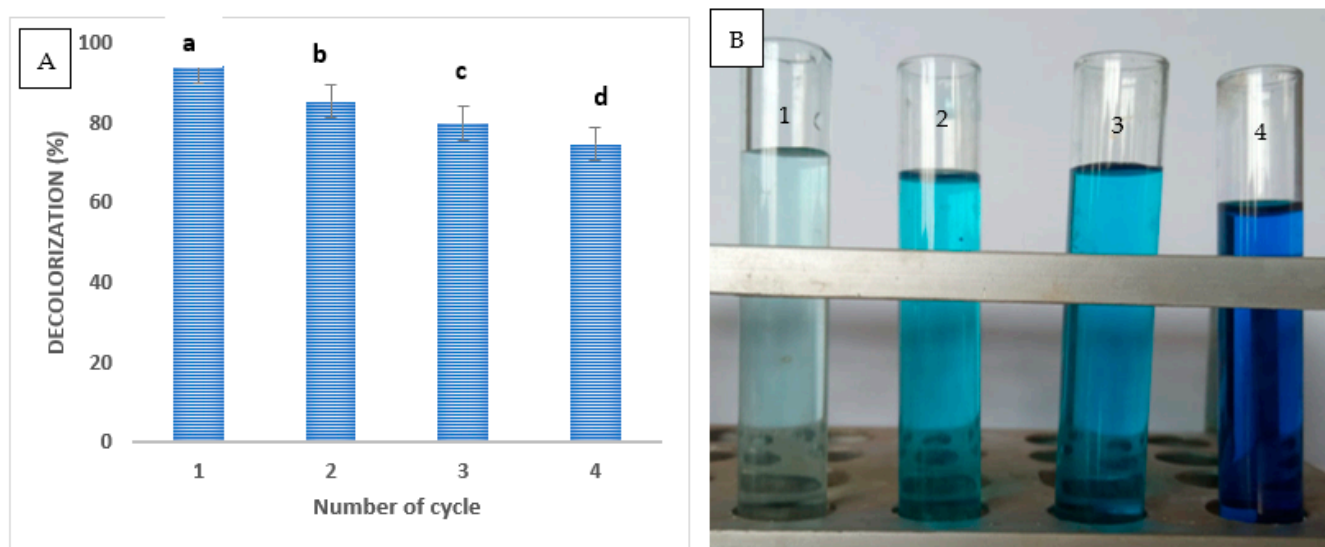


Figure 7. (A) ZnONPs recycling in methylene blue removal process; (B) At cycles 1–4 of the methylene blue removal cycle, the color changes. Letters a, b, c and d mean significance power.

2.6. Comparison between ZnO and Other Solid Adsorbents and Photocatalysts

A comparison of the photocatalytic activities for ZnO and other published nano-materials is presented in Table 2 [92–97]. Based on the tabulated data for photocatalytic degradation of methylene blue, we can conclude that nano zinc oxide and Other solid adsorbents are used in environmental applications.

Table 2. Photocatalytic degradation of methylene blue dye using ZnONPs and modified ZnONPs.

Type of Nanomaterial	Type of Dye	Photocatalysis	References
In/ZnO nanoparticles	methylene blue	89%	[92]
ZnO/C	methylene blue	95%	[95]
ZnONPs	methylene blue	92.5%	[93]
Ag-ZnO/g-C ₃ N ₄ /GO nanocomposite	methylene blue	93.43%	[94]
N-doped ZnO	methylene blue	95.3%	[97]
Gd-doped ZnO nanoparticles	methylene blue	93%	[96]

3. Materials and Methods

3.1. Materials

Zinc acetate dihydrate ($\text{Zn}(\text{CH}_3\text{COO})_2 \cdot 2\text{H}_2\text{O}$), methylene blue, and sodium hydroxide (NaOH) were analytical-grade compounds that were purchased from Sigma-Aldrich for use in this research.

3.2. Preparation of *P. indica* Leaf Extract

Pluchea indica leaves were obtained from Egypt's Giza Governorate. The recovered leaves were thoroughly cleansed with double-distilled water and left to dry for 5 days to eliminate any contaminants. Next, 5 g of the chopped material was combined with 100 mL of deionized water to create the extract, which was then heated at 65 °C for 60 min before being decanted. For use within a week, the supernatant was centrifuged for 10 min at 10,000 rpm and stored at 4 °C [98].

3.3. Biosynthesis of ZnONPs Using Leaf Extracts of *P. indica*

To biosynthesize ZnONPs, zinc acetate (3 mM) was added to *P. indica* leaf extract and agitated at 150 rpm for 24 h at 30 °C. At the end of the incubation period, a white tint was seen as a result of ZnONPs production. Drying the ZnONPs took 48 h at 80 °C. The ZnONPs product was eventually gathered and put through additional testing (Figure 8).

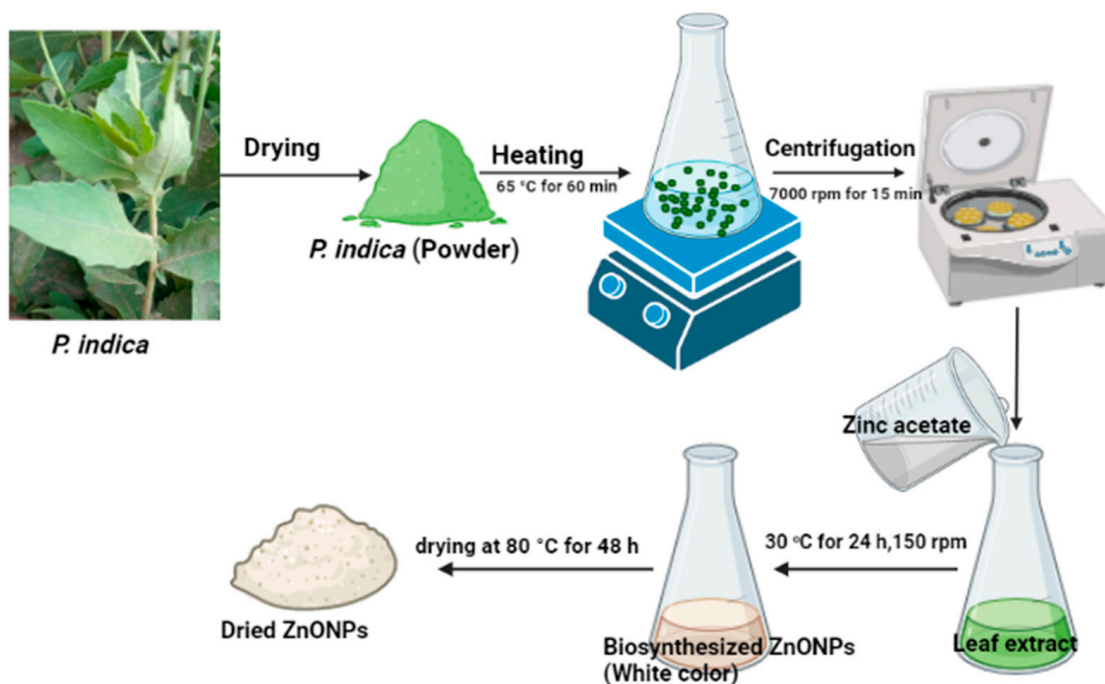


Figure 8. Preparation of *P. indica* leaf extract and biosynthesis of ZnONPs.

3.4. Characterization of ZnONPs

The characterization of ZnONPs was performed using Ultraviolet-visible (UV-vis) spectra, and the development of ZnONPs was tracked by observing changes in the color of the solution. UV-vis spectra were used to monitor the biosynthesis of ZnONPs in a colloid solution because surface plasmon stimulation causes it to produce a strong absorption peak. At wavelengths between 200 and 600 nm, the JENWAY 6305 Spectrophotometer was used to observe color change. The size and shape of nanoparticles were determined using a TEM (JEM-1230, Japan, Akishima, Tokyo 196-8558) and selected area electron diffraction (SAED). Using a Malvern Zetazier Instrument (Malvern, UK), DLS measurements were used to assess the particle size distribution of ZnONPs. The energy dispersive spectroscopy (EDX) apparatus (JEOL, JSM-6360LA, Tokyo, Japan) was coupled to a scanning electron microscope (SEM), which was used to examine the elemental composition of mycosynthesized ZnONPs. The potential biomolecules included in biosynthesized ZnONPs were identified using FTIR. The material was scanned using a Fourier Transform-Infrared Spectrometer (Agilent System Cary 660 FTIR model) in the infrared region of 400–4000 cm^{-1} . X-ray diffraction patterns were analyzed using the X'Pert Pro X-ray diffractometer (Philips, Eindhoven, Netherlands). The average crystallite size of ZnONPs may also be calculated using the Debye–Scherrer equation. ZnONPs' crystalline structure was identified in the 2θ range of 10° to 80°.

3.5. Antimicrobial Activity

Biosynthesized ZnONPs were evaluated for antimicrobial activity toward Gram-negative bacteria (*Escherichia coli* ATCC 25922 and *Pseudomonas aeruginosa* ATCC 27853), Gram-positive bacteria (*Enterococcus faecalis* ATCC 29212, *Staphylococcus aureus* ATCC 25923 and *Bacillus subtilis* ATCC 6051) and unicellular fungi (*Candida albicans* ATCC 90028 and *Cryptococcus neoformans* ATCC 14116). Minor modifications were made to the Clinical

Laboratory Standard Institute's guideline M51-A2 [99] when performing the diffusion in agar test. Individually, 100 μL of ZnONPs, leaf extract, standard antibiotic (Ampicillin/sulbactam), reference antifungal (Nystatin), and zinc acetate at a concentration of 1000 $\mu\text{g}/\text{mL}$ were added to the agar well, and then plates were put in the refrigerator for 2 h followed by incubation at (37 $^{\circ}\text{C}$ for 24 h)/(30 $^{\circ}\text{C}$ for 48 h) for bacterial/fungal strains, respectively. Then, inhibition-zone diameters were measured. ZnONPs and AMC/FLU were prepared at a variety of concentrations ranging from 1000 to 3.9 g/mL , and their respective MICs were then tested against a number of bacterial and fungal strains [100,101].

3.6. Photocatalytic Activity

The catalytic activity of biosynthesized ZnONPs was examined using methylene blue under both dark and light stimulation. The experiment involved mixing 50 mL of MB solution with various amounts of ZnONPs (25, 50, 75, and 100 mg) over a range of contact periods (30, 60, 90, 120, 150, 180, 240, and 300 min). A 250-watt halogen lamp served as the illumination source. Briefly, 50 mL of the MB solution was added to a specified ZnONPs concentration after the MB solution had been made at a concentration of 10 mg L^{-1} . Earlier in the experiment, the prior mixture was agitated for 30 min to reach the balance of absorption and desorption. The mixture was then exposed to light and incubated at room temperature with aeration. For comparison analysis, the same experiment was carried out once again under identical circumstances under dark irradiation. The optical density of the clear supernatant was measured using spectrophotometers, M-ETCAL, OK International Ltd., Eastleigh, UK, at λ max of MB (663 nm), after 2.0 mL of each treatment had been centrifuged at 5000 rpm for 10 min [102]. The following calculation was used to compute the decolorization percentages of MB color removal:

$$D\% = ((\text{dye 1} - \text{dye 2})/\text{dye 1}) \times 100$$

where D% represents the ratio of decolorization, dye (1) represents starting absorbance, and dye (2) represents final absorbance. For the fourth cycle, the catalyst's reusability in the degradation of MB was accomplished under ideal circumstances. The catalyst from the first cycle was recovered by centrifugation, subjected to two washings with distilled water, and then oven-dried at 80 $^{\circ}\text{C}$ to minimize water content before being used in the second cycle.

3.7. Statistical Analysis

All results presented in this study are the mean of three independent replicates. The SPSS v17 statistical software was used to analyze variance in the data. The mean difference between the treatments was analyzed by the Tukey HSD test at a significant level of $p \leq 0.05$.

4. Conclusions

In this study, *P. indica* leaf extract was used, for the first time, to synthesize ZnONPs utilizing a simple, effective, and eco-friendly method. The size, shape, and structure of the biosynthesized NPs were evaluated using transmission electron microscopy, Fourier transform-infrared spectroscopy, X-ray diffractometry, and dynamic light scattering investigations. Broad XRD peaks were present in the biosynthesized ZnONPs, confirming their nanocrystallinity and average size of 21.9 nm. The capping activity on the surface of ZnONPs is supported by the presence of polyphenols' stretching vibrations, which are present in the extract. The ZnONPs were observed at 360 nm. The biosynthesized ZnONPs exhibited antibacterial and antifungal activity against Gram-positive, Gram-negative, and unicellular fungi. The ZnONPs were found to have high efficacy in dye removal and to be simple to reuse four times. The highest dye decolorization was 95% after 150 min. Our findings highlight the significance of choosing the right plant to produce a particular NP shape in relation to the characteristics and potential uses of biosynthesized nanoparticles.

Author Contributions: Conceptualization, A.H.H.; methodology, A.H.H., A.A.A.-A., E.S.; software, N.I.E.; validation, A.H.H., A.A.A.-A., N.I.E., E.S.; formal analysis, A.H.H., E.S.; investigation, N.I.E.; resources, A.H.H., A.A.A.-A., N.I.E., E.S.; data curation, A.H.H., A.A.A.-A., N.I.E., E.S.; writing—original draft preparation, A.H.H., A.A.A.-A., E.S.; writing—review and editing, A.H.H., A.A.A.-A., N.I.E., E.S.; funding acquisition, A.A.A.-A. All authors have read and agreed to the published version of the manuscript.

Funding: The authors extend their appreciation to the researcher supporting project number (RSP2023R505), King Saud University, Riyadh, Saudi Arabia, for funding this work.

Institutional Review Board Statement: All authors approved.

Informed Consent Statement: All authors agree to publication.

Data Availability Statement: All data and materials are viable.

Acknowledgments: The authors would like to thank the Botany and Microbiology Department, Faculty of Science, Al-Azhar University. Moreover, the authors extend their appreciation to the researcher supporting project number (RSP2023R505), King Saud University, Riyadh, Saudi Arabia, for funding this work.

Conflicts of Interest: The authors declare no conflict of interest.

Sample Availability: Not applicable.

References

1. Parvin, F.; Islam, S.; Akm, S.I.; Urmy, Z.; Ahmed, S. A study on the solutions of environment pollutions and worker's health problems caused by textile manufacturing operations. *Biomed. J. Sci. Tech. Res.* **2020**, *28*, 21831–21844. [[CrossRef](#)]
2. Solayman, H.; Hossen, A.; Aziz, A.A.; Yahya, N.Y.; Leong, K.H.; Sim, L.C.; Monir, M.U.; Zoh, K.-D. Performance Evaluation of Dye Wastewater Treatment Technologies: A Review. *J. Environ. Chem. Eng.* **2023**, *11*, 109610. [[CrossRef](#)]
3. Sahoo, J.K.; Hota, A.; Singh, C.; Barik, S.; Sahu, N.; Sahoo, S.K.; Sahu, M.K.; Sahoo, H. Rice husk and rice straw based materials for toxic metals and dyes removal: A comprehensive and critical review. *Int. J. Environ. Anal. Chem.* **2021**, *1–23*, in press. [[CrossRef](#)]
4. Oladoye, P.O.; Ajiboye, T.O.; Omotola, E.O.; Oyewola, O.J. Methylene blue dye: Toxicity and potential technologies for elimination from (waste) water. *Results Eng.* **2022**, *16*, 100678. [[CrossRef](#)]
5. Haleem, A.; Pan, J.-M.; Shah, A.; Hussain, H.; He, W.-D. A systematic review on new advancement and assessment of emerging polymeric cryogels for environmental sustainability and energy production. *Sep. Purif. Technol.* **2023**, *316*, 123678. [[CrossRef](#)]
6. Khan, M.D.; Singh, A.; Tabraiz, S.; Sheikh, J. Current perspectives, recent advancements, and efficiencies of various dye-containing wastewater treatment technologies. *J. Water Process. Eng.* **2023**, *53*, 103579. [[CrossRef](#)]
7. Cwalinski, T.; Polom, W.; Marano, L.; Roviello, G.; D'angelo, A.; Cwalina, N.; Matuszewski, M.; Roviello, F.; Jaskiewicz, J.; Polom, K. Methylene blue—Current knowledge, fluorescent properties, and its future use. *J. Clin. Med.* **2020**, *9*, 3538. [[CrossRef](#)]
8. Wang, M.; Xu, Z.; Qi, Z.; Cai, Y.; Li, G.; Choi, W.; An, T. Repeated photocatalytic inactivation of *E. coli* by UV+ Ni foam@ TiO₂: Performance and photocatalyst deactivation. *Chem. Eng. J.* **2023**, *468*, 143680. [[CrossRef](#)]
9. Mohapatra, R.K.; Behera, S.S.; Patra, J.K.; Thatoi, H.; Parhi, P.K. Potential application of bacterial biofilm for bioremediation of toxic heavy metals and dye-contaminated environments. In *New and Future Developments in Microbial Biotechnology and Bioengineering: Microbial Biofilms*; Elsevier: Amsterdam, The Netherlands, 2020; pp. 267–281. [[CrossRef](#)]
10. Al-Tohamy, R.; Ali, S.S.; Li, F.; Okasha, K.M.; Mahmoud, Y.A.-G.; Elsamahy, T.; Jiao, H.; Fu, Y.; Sun, J. A critical review on the treatment of dye-containing wastewater: Ecotoxicological and health concerns of textile dyes and possible remediation approaches for environmental safety. *Ecotoxicol. Environ. Saf.* **2022**, *231*, 113160. [[CrossRef](#)]
11. Haleem, A.; Shafiq, A.; Chen, S.-Q.; Nazar, M. A Comprehensive Review on Adsorption, Photocatalytic and Chemical Degradation of Dyes and Nitro-Compounds over Different Kinds of Porous and Composite Materials. *Molecules* **2023**, *28*, 1081. [[CrossRef](#)]
12. Aragaw, T.A.; Bogale, F.M. Biomass-based adsorbents for removal of dyes from wastewater: A review. *Front. Environ. Sci.* **2021**, *9*, 558. [[CrossRef](#)]
13. Dutt, M.A.; Hanif, M.A.; Nadeem, F.; Bhatti, H.N. A review of advances in engineered composite materials popular for wastewater treatment. *J. Environ. Chem. Eng.* **2020**, *8*, 104073. [[CrossRef](#)]
14. Jaison, A.; Mohan, A.; Lee, Y.-C. Recent Developments in Photocatalytic Nanotechnology for Purifying Air Polluted with Volatile Organic Compounds: Effect of Operating Parameters and Catalyst Deactivation. *Catalysts* **2023**, *13*, 407. [[CrossRef](#)]
15. Anawar, H.; Chowdhury, R. Remediation of polluted river water by biological, chemical, ecological and engineering processes. *Sustainability* **2020**, *12*, 7017. [[CrossRef](#)]
16. Madkour, L.H. Introduction to nanotechnology (NT) and nanomaterials (NMs). In *Nanoelectronic Materials*; Springer: Cham, Switzerland, 2019; pp. 1–47. [[CrossRef](#)]
17. Haleem, A.; Chen, S.; Pan, J.; Weidong, H. Gamma radiation induced synthesis of double network hydrophilic cryogels at low pH loaded with AuNPs for fast and efficient degradation of Congo red. *J. Hazard. Mater. Adv.* **2023**, *10*, 100299. [[CrossRef](#)]

18. Abdelaziz, A.M.; Salem, S.S.; Khalil, A.M.A.; El-Wakil, D.A.; Fouda, H.M.; Hashem, A.H. Potential of biosynthesized zinc oxide nanoparticles to control Fusarium wilt disease in eggplant (*Solanum melongena*) and promote plant growth. *Biometals* **2022**, *35*, 601–616. [[CrossRef](#)] [[PubMed](#)]
19. Hasanin, M.; Hashem, A.H.; Lashin, I.; Hassan, S.A.M. In vitro improvement and rooting of banana plantlets using antifungal nanocomposite based on myco-synthesized copper oxide nanoparticles and starch. *Biomass Convers. Biorefinery* **2021**, *in press*. [[CrossRef](#)]
20. Hashem, A.H.; Al Abboud, M.A.; Alawlaqi, M.M.; Abdelghany, T.M.; Hasanin, M. Synthesis of nanocapsules based on biosynthesized nickel nanoparticles and potato starch: Antimicrobial, antioxidant, and anticancer activity. *Starch-Stärke* **2022**, *74*, 2100165. [[CrossRef](#)]
21. El-Naggar, M.E.; Hasanin, M.; Hashem, A.H. Eco-Friendly Synthesis of Superhydrophobic Antimicrobial Film Based on Cellulose Acetate/Polycaprolactone Loaded with the Green Biosynthesized Copper Nanoparticles for Food Packaging Application. *J. Polym. Environ.* **2022**, *30*, 1820–1832. [[CrossRef](#)]
22. Hashem, A.H.; Selim, T.A.; Alruhaili, M.H.; Selim, S.; Alkhalifah, D.H.M.; Al Jaouni, S.K.; Salem, S.S. Unveiling Antimicrobial and Insecticidal Activities of Biosynthesized Selenium Nanoparticles Using Prickly Pear Peel Waste. *J. Funct. Biomater.* **2022**, *13*, 112. [[CrossRef](#)]
23. Ali, O.M.; Hasanin, M.S.; Suleiman, W.B.; Helal, E.E.-H.; Hashem, A.H. Green biosynthesis of titanium dioxide quantum dots using watermelon peel waste: Antimicrobial, antioxidant, and anticancer activities. *Biomass Convers. Biorefinery* **2022**, *1–12*, *in press*. [[CrossRef](#)]
24. Saied, E.; Hashem, A.H.; Ali, O.M.; Selim, S.; Almuhayawi, M.S.; Elbahnasawy, M.A. Photocatalytic and Antimicrobial Activities of Biosynthesized Silver Nanoparticles Using *Cytobacillus firmus*. *Life* **2022**, *12*, 1331. [[CrossRef](#)] [[PubMed](#)]
25. Hashem, A.H.; Saied, E.; Amin, B.H.; Alotibi, F.O.; Al-Askar, A.A.; Arishi, A.A.; Elkady, F.M.; Elbahnasawy, M.A. Antifungal Activity of Biosynthesized Silver Nanoparticles (AgNPs) against *Aspergilli* Causing Aspergillosis: Ultrastructure Study. *J. Funct. Biomater.* **2022**, *13*, 242. [[CrossRef](#)]
26. Findik, F. Nanomaterials and their applications. *Period. Eng. Nat. Sci.* **2021**, *9*, 62–75. [[CrossRef](#)]
27. Muhammad, S.F. Nanotechnology Particle Characteristic. Bachelor's Thesis, Salahaddin University-Erbil, Erbil, Iraq, 2021.
28. Bushra, R.; Mohamad, S.; Alias, Y.; Jin, Y.; Ahmad, M. Current approaches and methodologies to explore the perceptive adsorption mechanism of dyes on low-cost agricultural waste: A review. *Microporous Mesoporous Mater.* **2021**, *319*, 111040. [[CrossRef](#)]
29. Shokry, H.; Elkady, M.; Hamad, H. Nano activated carbon from industrial mine coal as adsorbents for removal of dye from simulated textile wastewater: Operational parameters and mechanism study. *J. Mater. Res. Technol.* **2019**, *8*, 4477–4488. [[CrossRef](#)]
30. Uddin, T.M.; Chakraborty, A.J.; Khushro, A.; Zidan, B.R.M.; Mitra, S.; Bin Emran, T.; Dhama, K.; Ripon, K.H.; Gajdacs, M.; Sahibzada, M.U.K.; et al. Antibiotic resistance in microbes: History, mechanisms, therapeutic strategies and future prospects. *J. Infect. Public Health* **2021**, *14*, 1750–1766. [[CrossRef](#)]
31. Saleem, A.; Naureen, I.; Tasleem, G.; Anwar, R.; Mairaj, M.; Muddassar, H.; Rana, N.J. Microbial Assisted Bioremediation of Polluted Water. *Haya: Saudi J. Life Sci.* **2022**, *7*, 116–127. [[CrossRef](#)]
32. Rambabu, K.; Bharath, G.; Banat, F.; Show, P.L. Green synthesis of zinc oxide nanoparticles using Phoenix dactylifera waste as bioreductant for effective dye degradation and antibacterial performance in wastewater treatment. *J. Hazard. Mater.* **2021**, *402*, 123560. [[CrossRef](#)]
33. Adimule, V.M.; Nandi, S.S.; Kerur, S.S.; Khadapure, S.A.; Chinnam, S. Recent advances in the one-pot synthesis of coumarin derivatives from different starting materials using nanoparticles: A Review. *Top. Catal.* **2022**, *1–31*, *in press*. [[CrossRef](#)]
34. Chakraborty, I.; Pandey, A. A review article on application of ZnO-based nanocomposite materials in environmental remediation. *Mater. Today: Proc.* **2023**, *in press*.
35. Mandal, A.K.; Katuwal, S.; Tettey, F.; Gupta, A.; Bhattarai, S.; Jaisi, S.; Bhandari, D.P.; Shah, A.K.; Bhattarai, N.; Parajuli, N. Current research on zinc oxide nanoparticles: Synthesis, characterization, and biomedical applications. *Nanomaterials* **2022**, *12*, 3066. [[CrossRef](#)]
36. Ibrahim, S.R.M.; Bagalagel, A.A.; Diri, R.M.; Noor, A.O.; Bakhsh, H.T.; Mohamed, G.A. Phytoconstituents and pharmacological activities of indian camphorweed (*Pluchea indica*): A multi-potential medicinal plant of nutritional and ethnomedicinal importance. *Molecules* **2022**, *27*, 2383. [[CrossRef](#)]
37. Chiangnoon, R.; Samee, W.; Uttayarat, P.; Jittachai, W.; Ruksiriwanich, W.; Sommano, S.R.; Athikomkulchai, S.; Chittasupho, C. Phytochemical Analysis, Antioxidant, and Wound Healing Activity of *Pluchea indica* L.(Less) Branch Extract Nanoparticles. *Molecules* **2022**, *27*, 635. [[CrossRef](#)]
38. Pranata, N.; Boli, G.E.D.; Sinta, R.; Sugiaman, V.K. Effect of beluntas leaf extract (*Pluchea indica*) on oral mucosal wound healing in terms of density of inflammatory cells and collagen. *Syst. Rev. Pharm.* **2021**, *12*, 618–622.
39. Iravani, S. Green synthesis of metal nanoparticles using plants. *Green Chem.* **2011**, *13*, 2638–2650. [[CrossRef](#)]
40. Singh, J.; Dutta, T.; Kim, K.-H.; Rawat, M.; Samddar, P.; Kumar, P. 'Green' synthesis of metals and their oxide nanoparticles: Applications for environmental remediation. *J. Nanobiotechnol.* **2018**, *16*, 84. [[CrossRef](#)]
41. Ovais, M.; Khalil, A.T.; Islam, N.U.; Ahmad, I.; Ayaz, M.; Saravanan, M.; Shinwari, Z.K.; Mukherjee, S. Role of plant phytochemicals and microbial enzymes in biosynthesis of metallic nanoparticles. *Appl. Microbiol. Biotechnol.* **2018**, *102*, 6799–6814. [[CrossRef](#)]

42. Nair, G.M.; Sajini, T.; Mathew, B. Advanced green approaches for metal and metal oxide nanoparticles synthesis and their environmental applications. *Talanta Open* **2021**, *5*, 100080. [[CrossRef](#)]
43. Kanagamani, K.; Muthukrishnan, P.; Saravanakumar, K.; Shankar, K.; Kathiresan, A. Photocatalytic degradation of environmental perilous gentian violet dye using leucaena-mediated zinc oxide nanoparticle and its anticancer activity. *Rare Met.* **2019**, *38*, 277–286. [[CrossRef](#)]
44. Lashin, I.; Hasanin, M.; Hassan, S.A.M.; Hashem, A.H. Green biosynthesis of zinc and selenium oxide nanoparticles using callus extract of *Ziziphus spina-christi*: Characterization, antimicrobial, and antioxidant activity. *Biomass Convers. Biorefinery* **2021**, 1–14, *in press*. [[CrossRef](#)]
45. Majhi, J.K.; Kuri, P.K.J. Enhancement of spectral shift of plasmon resonances in bimetallic noble metal nanoparticles in core-shell structure. *J. Nanoparticle Res.* **2020**, *22*, 86. [[CrossRef](#)]
46. Mani, V.M.; Nivetha, S.; Sabarathinam, S.; Barath, S.; Das, M.A.; Basha, S.; Elfasakhany, A.; Pugazhendhi, A. Multifunctionalities of mycosynthesized zinc oxide nanoparticles (ZnONPs) from *Cladosporium tenuissimum* FCBG: Antimicrobial additives for paints coating, functionalized fabrics and biomedical properties. *Prog. Org. Coat.* **2022**, *163*, 106650. [[CrossRef](#)]
47. Azim, Z.; Singh, N.; Khare, S.; Singh, A.; Amist, N.; Niharika; Yadav, R.K. Green synthesis of zinc oxide nanoparticles using *Vernonia cinerea* leaf extract and evaluation as nano-nutrient on the growth and development of tomato seedling. *Plant Nano Biol.* **2022**, *2*, 100011. [[CrossRef](#)]
48. Kumar, R.; Vinoth, S.; Baskar, V.; Arun, M.; Gurusaravanan, P. Synthesis of zinc oxide nanoparticles mediated by *Dictyota dichotoma* endophytic fungi and its photocatalytic degradation of fast green dye and antibacterial applications. *S. Afr. J. Bot.* **2022**, *151*, 337–344. [[CrossRef](#)]
49. Vijayakumar, N.; Bhuvaneshwari, V.K.; Ayyadurai, G.K.; Jayaprakash, R.; Gopinath, K.; Nicoletti, M.; Alarifi, S.; Govindarajan, M. Green synthesis of zinc oxide nanoparticles using *Anoectochilus elatus*, and their biomedical applications. *Saudi J. Biol. Sci.* **2021**, *29*, 2270–2279. [[CrossRef](#)]
50. Shubha, J.P.; Kavalli, K.; Adil, S.F.; Assal, M.E.; Hatshan, M.R.; Dubasi, N. Facile green synthesis of semiconductive ZnO nanoparticles for photocatalytic degradation of dyes from the textile industry: A kinetic approach. *J. King Saud Univ. Sci.* **2022**, *34*, 102047. [[CrossRef](#)]
51. Abdo, A.M.; Fouda, A.; Eid, A.M.; Fahmy, N.M.; Elsayed, A.M.; Khalil, A.M.A.; Alzahrani, O.M.; Ahmed, A.F.; Soliman, A.M. Green synthesis of Zinc Oxide Nanoparticles (ZnO-NPs) by *Pseudomonas aeruginosa* and their activity against pathogenic microbes and common house mosquito, *Culex pipiens*. *Materials* **2021**, *14*, 6983. [[CrossRef](#)] [[PubMed](#)]
52. Mohamed, A.A.; Fouda, A.; Abdel-Rahman, M.A.; Hassan, S.E.-D.; El-Gamal, M.S.; Salem, S.S.; Shaheen, T.I. Fungal strain impacts the shape, bioactivity and multifunctional properties of green synthesized zinc oxide nanoparticles. *Biocatal. Agric. Biotechnol.* **2019**, *19*, 101103. [[CrossRef](#)]
53. Abdelkader, D.H.; Negm, W.A.; Elekhawy, E.; Eliwa, D.; Aldosari, B.N.; Almurshedi, A.S. Zinc oxide nanoparticles as potential delivery carrier: Green synthesis by *Aspergillus niger* endophytic fungus, characterization, and in vitro/in vivo antibacterial activity. *Pharmaceuticals* **2022**, *15*, 1057. [[CrossRef](#)] [[PubMed](#)]
54. Kulkarni, P.; Ramakrishna, K.J. Biosynthesis of zinc oxide nanoparticles by endophytic fungi *aspergillus niger* and their potential antibacterial effects on *propionibacterium acnes*. *J. Adv. Sci. Res.* **2020**, *11*, 178–183.
55. Rasha, E.; Alkhulaifi, M.M.; AlOthman, M.; Khalid, I.; Doaa, E.; Alaa, K.; Awad, M.A.; Abdalla, M. Effects of zinc oxide nanoparticles synthesized using *aspergillus niger* on carbapenem-resistant *klebsiella pneumonia* in vitro and in vivo. *Front. Cell. Infect. Microbiol.* **2021**, *11*, 748739. [[CrossRef](#)]
56. Mekky, A.E.; Farrag, A.A.; Hmed, A.A.; Sofy, A.R. Preparation of zinc oxide nanoparticles using *aspergillus niger* as antimicrobial and anticancer agents. *J. Pure Appl. Microbiol.* **2021**, *15*, 1547–1566. [[CrossRef](#)]
57. Fagier, M.A.J. Plant-mediated biosynthesis and photocatalysis activities of zinc oxide nanoparticles: A prospect towards dyes mineralization. *J. Nanotechnol.* **2021**, *2021*, 6629180. [[CrossRef](#)]
58. Dias, C.; Ayyanar, M.; Amalraj, S.; Khanal, P.; Subramaniyan, V.; Das, S.; Gandhale, P.; Biswa, V.; Ali, R.; Gurav, N.; et al. Biogenic synthesis of zinc oxide nanoparticles using mushroom fungus *Cordyceps militaris*: Characterization and mechanistic insights of therapeutic investigation. *J. Drug Deliv. Sci. Technol.* **2022**, *73*, 103444. [[CrossRef](#)]
59. Al-Dhabi, N.A.; Arasu, M.V. Environmentally-friendly green approach for the production of zinc oxide nanoparticles and their anti-fungal, ovicidal, and larvicidal properties. *Nanomaterials* **2018**, *8*, 500. [[CrossRef](#)]
60. Rajivgandhi, G.; Gnanamangai, B.M.; Prabha, T.H.; Poornima, S.; Maruthupandy, M.; Alharbi, N.S.; Kadaikunnan, S.; Li, W.-J. Biosynthesized zinc oxide nanoparticles (ZnO NPs) using actinomycetes enhance the anti-bacterial efficacy against *K. Pneumoniae*. *J. King Saud Univ. Sci.* **2022**, *34*, 101731. [[CrossRef](#)]
61. Fouda, A.; Eid, A.M.; Abdelkareem, A.; Said, H.A.; El-Belely, E.F.; Alkhalifah, D.H.M.; Alshallash, K.S.; Hassan, S.E.-D. Phyco-Synthesized zinc oxide nanoparticles using marine macroalgae, *Ulva fasciata* delile, characterization, antibacterial activity, photocatalysis, and tanning wastewater treatment. *Catalysts* **2022**, *12*, 756. [[CrossRef](#)]
62. Javed, R.; Zia, M.; Naz, S.; Aisida, S.O.; Ain, N.U.; Ao, Q. Role of capping agents in the application of nanoparticles in biomedicine and environmental remediation: Recent trends and future prospects. *J. Nanobiotechnol.* **2020**, *18*, 172. [[CrossRef](#)] [[PubMed](#)]
63. Aziz, A.; Memon, Z.; Bhutto, A. Efficient photocatalytic degradation of industrial wastewater dye by *Grewia asiatica* mediated zinc oxide nanoparticles. *Optik* **2023**, *272*, 170352. [[CrossRef](#)]

64. Fouda, A.; Saad, E.; Salem, S.S.; Shaheen, T.I. In-Vitro cytotoxicity, antibacterial, and UV protection properties of the biosynthesized Zinc oxide nanoparticles for medical textile applications. *Microb. Pathog.* **2018**, *125*, 252–261. [[CrossRef](#)] [[PubMed](#)]
65. Raj, L.F.A.A.; Jayalakshmy, E. Biosynthesis and characterization of zinc oxide nanoparticles using root extract of zingiber officinale. *Orient. J. Chem.* **2015**, *31*, 51–56. [[CrossRef](#)]
66. Mohamed, A.A.; Abu-Elghait, M.; Ahmed, N.E.; Salem, S.S. Eco-friendly mycogenic synthesis of zno and cuo nanoparticles for in vitro antibacterial, antibiofilm, and antifungal applications. *Biol. Trace Elem. Res.* **2020**, *199*, 2788–2799. [[CrossRef](#)] [[PubMed](#)]
67. Naseer, M.; Aslam, U.; Khalid, B.; Chen, B. Green route to synthesize Zinc Oxide Nanoparticles using leaf extracts of Cassia fistula and Melia azadarach and their antibacterial potential. *Sci. Rep.* **2020**, *10*, 9055. [[CrossRef](#)]
68. Iqbal, J.; Abbasi, B.A.; Yaseen, T.; Zahra, S.A.; Shahbaz, A.; Shah, S.A.; Uddin, S.; Ma, X.; Raouf, B.; Kanwal, S.; et al. Green synthesis of zinc oxide nanoparticles using Elaeagnus angustifolia L. leaf extracts and their multiple in vitro biological applications. *Sci. Rep.* **2021**, *11*, 20988. [[CrossRef](#)] [[PubMed](#)]
69. Santhoshkumar, J.; Kumar, S.V.; Rajeshkumar, S. Synthesis of zinc oxide nanoparticles using plant leaf extract against urinary tract infection pathogen. *Resour. Technol.* **2017**, *3*, 459–465. [[CrossRef](#)]
70. Gharpure, S.; Yadwade, R.; Mehmood, S.; Ankamwar, B. Antibacterial Activities of Biosynthesized ZnO Nanoparticles Using Leaf and Fruit Extracts of Neolamarckia cadamba. *J. Nanosci. Nanotechnol.* **2021**, *21*, 6168–6182. [[CrossRef](#)]
71. MuthuKathija, M.; Badhusha, M.S.M.; Rama, V. Green synthesis of zinc oxide nanoparticles using Pisonia Alba leaf extract and its antibacterial activity. *Appl. Surf. Sci. Adv.* **2023**, *15*, 100400. [[CrossRef](#)]
72. Chaudhary, A.; Kumar, N.; Kumar, R.; Salar, R.K. Antimicrobial activity of zinc oxide nanoparticles synthesized from Aloe vera peel extract. *SN Appl. Sci.* **2018**, *1*, 136. [[CrossRef](#)]
73. Bala, N.; Saha, S.; Chakraborty, M.; Maiti, M.; Das, S.; Basu, R.; Nandy, P. Green synthesis of zinc oxide nanoparticles using Hibiscus subdariffa leaf extract: Effect of temperature on synthesis, anti-bacterial activity and anti-diabetic activity. *RSC Adv.* **2015**, *5*, 4993–5003. [[CrossRef](#)]
74. Urge, S.K.; Dibaba, S.T.; Gemta, A.B. Green Synthesis Method of ZnO Nanoparticles using Extracts of *Zingiber officinale* and Garlic Bulb (*Allium sativum*) and Their Synergetic Effect for Antibacterial Activities. *J. Nanomater.* **2023**, *2023*, 7036247. [[CrossRef](#)]
75. Sirelkhatim, A.; Mahmud, S.; Seeni, A.; Kaus, N.H.M.; Ann, L.C.; Bakhori, S.K.M.; Hasan, H.; Mohamad, D. Review on Zinc Oxide Nanoparticles: Antibacterial Activity and Toxicity Mechanism. *Nano-Micro Lett.* **2015**, *7*, 219–242. [[CrossRef](#)] [[PubMed](#)]
76. Dwivedi, S.; Wahab, R.; Khan, F.; Mishra, Y.K.; Musarrat, J.; Al-Khedhairi, A.A. Reactive oxygen species mediated bacterial biofilm inhibition via zinc oxide nanoparticles and their statistical determination. *PLoS ONE* **2014**, *9*, e111289. [[CrossRef](#)]
77. Yuan, L.; Wang, Y.; Wang, J.; Xiao, H.; Liu, X. Additive effect of zinc oxide nanoparticles and isoorientin on apoptosis in human hepatoma cell line. *Toxicol. Lett.* **2014**, *225*, 294–304. [[CrossRef](#)] [[PubMed](#)]
78. Qumar, U.; Hassan, J.Z.; Bhatti, R.A.; Raza, A.; Nazir, G.; Nabgan, W.; Ikram, M. Photocatalysis vs adsorption by metal oxide nanoparticles. *J. Mater. Sci. Technol.* **2022**, *131*, 122–166. [[CrossRef](#)]
79. Saied, E.; Salem, S.S.; Al-Askar, A.A.; Elkady, F.M.; Arishi, A.A.; Hashem, A.H. Mycosynthesis of hematite (α -Fe₂O₃) nanoparticles using *Aspergillus niger* and their antimicrobial and photocatalytic activities. *Bioengineering* **2022**, *9*, 397. [[CrossRef](#)] [[PubMed](#)]
80. Rasool, A.; Kiran, S.; Gulzar, T.; Abrar, S.; Ghaffar, A.; Shahid, M.; Nosheen, S.; Naz, S. Biogenic synthesis and characterization of ZnO nanoparticles for degradation of synthetic dyes: A sustainable environmental cleaner approach. *J. Clean. Prod.* **2023**, *398*, 136616. [[CrossRef](#)]
81. Kapoor, R.T.; Danish, M.; Singh, R.S.; Rafatullah, M.; Hps, A.K. Exploiting microbial biomass in treating azo dyes contaminated wastewater: Mechanism of degradation and factors affecting microbial efficiency. *J. Water Process. Eng.* **2021**, *43*, 102255. [[CrossRef](#)]
82. Al-Arjan, W.S. Zinc oxide nanoparticles and their application in adsorption of toxic dye from aqueous solution. *Polymers* **2022**, *14*, 3086. [[CrossRef](#)]
83. Omran, A.M. Characterization of green route synthesized zinc oxide nanoparticles using Cyperus rotundus rhizome extract: Antioxidant, antibacterial, anticancer and photocatalytic potential. *J. Drug Deliv. Sci. Technol.* **2023**, *79*, 104000. [[CrossRef](#)]
84. Nguyen, N.T.T.; Nguyen, L.M.; Nguyen, T.T.T.; Nguyen, N.H.; Nguyen, D.H.; Nguyen, D.T.C.; Van Tran, T.J. Green synthesis of ZnFe₂O₄@ZnO nanocomposites using *Chrysanthemum* spp. floral waste for photocatalytic dye degradation. *J. Environ. Manag.* **2023**, *326*, 116746. [[CrossRef](#)]
85. Manojkumar, U.; Kaliannan, D.; Srinivasan, V.; Balasubramanian, B.; Kamyab, H.; Mussa, Z.H.; Palaniyappan, J.; Mesbah, M.; Chelliapan, S.; Palaninaicker, S. Green synthesis of zinc oxide nanoparticles using Brassica oleracea var. botrytis leaf extract: Photocatalytic, antimicrobial and larvicidal activity. *Chemosphere* **2023**, *323*, 138263. [[CrossRef](#)] [[PubMed](#)]
86. Mansour, A.T.; Alprol, A.E.; Khedawy, M.; Abualnaja, K.M.; Shalaby, T.A.; Rayan, G.; Ramadan, K.M.A.; Ashour, M. Green synthesis of zinc oxide nanoparticles using red seaweed for the elimination of organic toxic dye from an aqueous solution. *Materials* **2022**, *15*, 5169. [[CrossRef](#)] [[PubMed](#)]
87. Kaur, Y.; Jasrotia, T.; Kumar, R.; Chaudhary, G.R.; Chaudhary, S. Adsorptive removal of eriochrome black T (EBT) dye by using surface active low cost zinc oxide nanoparticles: A comparative overview. *Chemosphere* **2021**, *278*, 130366. [[CrossRef](#)] [[PubMed](#)]
88. Das, D.; Nandi, P. Ternary ZnCdSO composite photocatalyst for efficient dye degradation under visible light retaining Z-scheme of migration pathways for the photogenerated charge carriers. *Sol. Energy Mater. Sol. Cells* **2020**, *217*, 110674. [[CrossRef](#)]

89. Hunge, Y.; Yadav, A.; Kang, S.-W.; Kim, H. Facile synthesis of multitasking composite of Silver nanoparticle with Zinc oxide for 4-nitrophenol reduction, photocatalytic hydrogen production, and 4-chlorophenol degradation. *J. Alloys Compd.* **2022**, *928*, 167133. [[CrossRef](#)]
90. Akpomie, K.G.; Conradie, J.J.S.R. Synthesis, characterization, and regeneration of an inorganic–organic nanocomposite (ZnO@biomass) and its application in the capture of cationic dye. *Sci. Rep.* **2020**, *10*, 14441. [[CrossRef](#)]
91. Chauhan, A.K.; Kataria, N.; Garg, V. Green fabrication of ZnO nanoparticles using Eucalyptus spp. leaves extract and their application in wastewater remediation. *Chemosphere* **2020**, *247*, 125803. [[CrossRef](#)]
92. Baeissa, E. Photocatalytic degradation of methylene blue dye under visible light irradiation using In/ZnO nanocomposite. *Front. Nanosci. Nanotechnol.* **2016**, *2*, 1–5. [[CrossRef](#)]
93. Balcha, A.; Yadav, O.P.; Dey, T. Photocatalytic degradation of methylene blue dye by zinc oxide nanoparticles obtained from precipitation and sol-gel methods. *Environ. Sci. Pollut. Res.* **2016**, *23*, 25485–25493. [[CrossRef](#)]
94. Habibollahi, Z.; Peyravi, M.; Khalili, S.; Jahanshahi, M. ZnO-based ternary nanocomposite for decolorization of methylene blue by photocatalytic dynamic membrane. *Mater. Today Chem.* **2022**, *23*, 100748. [[CrossRef](#)]
95. Micheal, K.; Ayeshamariam, A.; Devanesan, S.; Bhuvaneshwari, K.; Pazhanivel, T.; AlSalhi, M.S.; Aljaafreh, M.J. Environmental friendly synthesis of carbon nanoplates supported ZnO nanorods for enhanced degradation of dyes and organic pollutants with visible light driven photocatalytic performance. *J. King Saud Univ. Sci.* **2019**, *32*, 1081–1087. [[CrossRef](#)]
96. Selvaraj, S.; Mohan, M.K.; Navaneethan, M.; Ponnusamy, S.; Muthamizhchelvan, C. Synthesis and photocatalytic activity of Gd doped ZnO nanoparticles for enhanced degradation of methylene blue under visible light. *Mater. Sci. Semicond. Process.* **2020**, *103*, 104622. [[CrossRef](#)]
97. Sun, L.; Shao, Q.; Zhang, Y.; Jiang, H.; Ge, S.; Lou, S.; Lin, J.; Zhang, J.; Wu, S.; Dong, M.; et al. N self-doped ZnO derived from microwave hydrothermal synthesized zeolitic imidazolate framework-8 toward enhanced photocatalytic degradation of methylene blue. *J. Colloid Interface Sci.* **2020**, *565*, 142–155. [[CrossRef](#)]
98. Molaei, R.; Farhadi, K.; Forough, M.; Pourhossein, A. Biosynthetic Route for the Preparation of Nonregular Gold Nanoparticles Using Aqueous Extracted of Nettle (*Urtica dioica* L.) Plant. *Synth. React. Inorg. Met. Nano-Met. Chem.* **2015**, *45*, 1489–1494. [[CrossRef](#)]
99. Rex, J.H. *Reference Method for Broth Dilution Antifungal Susceptibility Testing of Yeasts*; National Committee for Clinical Laboratory Standards: Wayne, PA, USA, 2002.
100. Valgas, C.; Souza, S.M.D.; Smânia, E.; Smânia, A. Screening methods to determine antibacterial activity of natural products. *Braz. J. Microbiol.* **2007**, *38*, 369–380. [[CrossRef](#)]
101. Dacrory, S.; Hashem, A.H.; Hasanin, M. Synthesis of cellulose based amino acid functionalized nano-biocomplex: Characterization, antifungal activity, molecular docking and hemocompatibility. *Environ. Nanotechnol. Monit. Manag.* **2021**, *15*, 100453. [[CrossRef](#)]
102. Alahdal, F.A.; Qashqoosh, M.T.; Manea, Y.K.; Salem, M.A.; Khan, A.M.; Naqvi, S. Eco-friendly synthesis of zinc oxide nanoparticles as nanosensor, nanocatalyst and antioxidant agent using leaf extract of *P. austroarabica*. *Opennano* **2022**, *8*, 100067. [[CrossRef](#)]

Disclaimer/Publisher’s Note: The statements, opinions and data contained in all publications are solely those of the individual author(s) and contributor(s) and not of MDPI and/or the editor(s). MDPI and/or the editor(s) disclaim responsibility for any injury to people or property resulting from any ideas, methods, instructions or products referred to in the content.